NANO EXPRESS

Interwell coupling effect in Si/SiGe quantum wells grown by ultra high vacuum chemical vapor deposition

Rui Wang · Soon Fatt Yoon · Fen Lu ·
Wei Jun Fan · Chong Yang Liu · Ter-Hoe Loh ·
Hoai Son Nguyen · Balasubramanian Narayanan

Abstract Si/Si$_{0.66}$Ge$_{0.34}$ coupled quantum well (CQW) structures with different barrier thickness of 40, 4 and 2 nm were grown on Si substrates using an ultra high vacuum chemical vapor deposition (UHV-CVD) system. The samples were characterized using high resolution x-ray diffraction (HRXRD), cross-sectional transmission electron microscopy (XTEM) and photoluminescence (PL) spectroscopy. Blue shift in PL peak energy due to interwell coupling was observed in the CQWs following increase in the Si barrier thickness. The Si/SiGe heterostructure growth process and theoretical band structure model was validated by comparing the energy of the no-phonon peak calculated by the 6 + 2-band $k \cdot p$ method with experimental PL data. Close agreement between theoretical calculations and experimental data was obtained.

Keywords Si/SiGe · Coupled quantum well · UHV-CVD

Introduction

Silicon is notably the most widely used semiconductor in the microelectronics industry. As such, the ability to realize light emitters based on silicon is a highly desirable goal that could lead to integrating optical and microelectronic functions on the same silicon-based platform. However, the indirect band characteristic of silicon prohibits the efficient radiative recombination of electrons and holes to result in coherent optical emission. Currently, there are a number of efforts to overcome this physical challenge, such as the use of Si nanocrystals and Er coupled Si [1–3]. Apart from these potential solutions, the quantum cascade (QC) structure is considered a promising method to realize a Si-based coherent light emitter. This is because the carrier transition mechanism for the QC structure is based on intersubband transition. Hence, the indirect band property of Si and SiGe alloy could be ignored.

Recently, intersubband photoluminescence (PL) and electroluminescence (EL) have been demonstrated in Si/SiGe QC structures [4–6]. Compared with other solutions, the emission wavelength of the QC emitter (QCE) lies at the mid- to far-infrared (also called terahertz) region, which is currently under utilized due to the lack of suitable material systems. In the QC structure, the active region is normally formed by the Si/SiGe superlattice layers, which comprise several layers of SiGe quantum wells (QWs) and Si barriers. In such a structure, interwell coupling effect plays an essential role to determine the energy transitions and resultant optical and electronic properties of the Si/SiGe QC structure. In other words, the intersubband transitions in the QC structures rely on the interwell coupling in the QWs. This is because the wave functions in the QC structures are no longer confined to a single well, but penetrate into barriers and extend over the entire region [7]. Therefore, the study of interwell coupling effect in the QWs remains a critical issue for

R. Wang · S. F. Yoon (✉) · F. Lu · W. J. Fan ·
C. Y. Liu
School of Electrical and Electronic Engineering, Nanyang Technological University, Nanyang Avenue, Singapore 639798, Singapore
e-mail: esfyoon@ntu.edu.sg

T.-H. Loh · H. S. Nguyen · B. Narayanan
Institute of Microelectronics, 11 Science Park Road
Singapore Science Park II, Singapore 117685, Singapore

realizing the QCE. Luminescence from CQWs in Si/SiGe materials grown by molecular beam epitaxy (MBE) has been reported by Fukatsu et al. [8–10]. However, in their reports, the Ge fraction in the SiGe QWs is less than 20%. This is not suitable for application in the QC structures, because the resulting valence band offset is only about 0.1 eV.

In this paper, we present a photoluminescence (PL) study on strained Si/Si$_{0.66}$Ge$_{0.34}$ CQWs grown by ultra high vacuum chemical vapor deposition (UHV-CVD). The Ge fraction in our SiGe QW samples is about twice the Ge fraction in the samples reported by Fukatsu et al. [8–10]. The higher Ge fraction in our samples is expected to produce an effectively larger valence band offset, which is more appropriate for design of the QC structure for light emission. The interwell coupling effect in the QC samples of different barrier thickness was investigated. Comparison with theoretical calculation of the energy transitions is presented.

Experimental details

The samples used in this study were grown in a UHV-CVD cold-wall 8-inch single-wafer epitaxy reactor. The chamber pressure is below 10^{-9} Pa. The reactant gases used for the deposition are disilane (Si$_2$H$_6$) and germane (GeH$_4$). P-type (boron doped at 2.5×10^{15} cm^{-3}) Si (100) substrates were cleaned using a standard solution comprising 10DI:2H$_2$O$_2$:1NH$_4$OH (by volume), then dipped into dilute HF (DHF) solution comprising 200H$_2$O:1HF for 2 min before deposition. Figure 1 shows the schematic diagrams of the structures and growth conditions of the three samples investigated in this study. A 3 nm-thick Si buffer layer was grown at 530°C at 1 nm/min on the p-type silicon substrate. This is followed by growth of the SiGe QWs, Si barriers and the Si cap layer. The SiGe QWs in sample 1 was deposited at 530°C at growth rate of 12 nm/min, while the Si barrier and cap layer were deposited at 600°C at 10 nm/min. In samples 2 and 3, the thin Si barriers between the two CQWs (4 nm and 2 nm, respectively) were grown under the same condition as the 3 nm-thick Si buffer layer. The thick Si barriers in sample 3 and the QWs and cap layers in both samples 2 and 3 were grown under the same condition as the barriers, the QWs and cap layer of sample 1, respectively. All the layers are nominally undoped.

Photoluminescence (PL) measurements were carried out at 4 K by exciting the sample using the 514.5 nm line from an Ar ion laser. The PL was detected by a
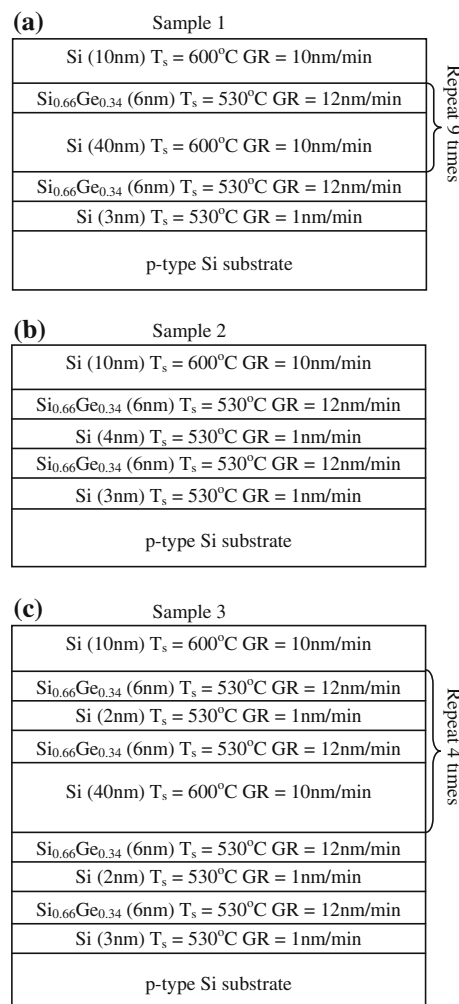

(a) Sample 1

| Si (10nm) T$_s$ = 600°C GR = 10nm/min |
| Si$_{0.66}$Ge$_{0.34}$ (6nm) T$_s$ = 530°C GR = 12nm/min |
| Si (40nm) T$_s$ = 600°C GR = 10nm/min |
| Si$_{0.66}$Ge$_{0.34}$ (6nm) T$_s$ = 530°C GR = 12nm/min |
| Si (3nm) T$_s$ = 530°C GR = 1nm/min |
| p-type Si substrate |

Repeat 9 times

(b) Sample 2

| Si (10nm) T$_s$ = 600°C GR = 10nm/min |
| Si$_{0.66}$Ge$_{0.34}$ (6nm) T$_s$ = 530°C GR = 12nm/min |
| Si (4nm) T$_s$ = 530°C GR = 1nm/min |
| Si$_{0.66}$Ge$_{0.34}$ (6nm) T$_s$ = 530°C GR = 12nm/min |
| Si (3nm) T$_s$ = 530°C GR = 1nm/min |
| p-type Si substrate |

(c) Sample 3

| Si (10nm) T$_s$ = 600°C GR = 10nm/min |
| Si$_{0.66}$Ge$_{0.34}$ (6nm) T$_s$ = 530°C GR = 12nm/min |
| Si (2nm) T$_s$ = 530°C GR = 1nm/min |
| Si$_{0.66}$Ge$_{0.34}$ (6nm) T$_s$ = 530°C GR = 12nm/min |
| Si (40nm) T$_s$ = 600°C GR = 10nm/min |
| Si$_{0.66}$Ge$_{0.34}$ (6nm) T$_s$ = 530°C GR = 12nm/min |
| Si (2nm) T$_s$ = 530°C GR = 1nm/min |
| Si$_{0.66}$Ge$_{0.34}$ (6nm) T$_s$ = 530°C GR = 12nm/min |
| Si (3nm) T$_s$ = 530°C GR = 1nm/min |
| p-type Si substrate |

Repeat 4 times

Fig. 1 Schematic diagrams of structures and growth conditions of samples 1, 2 and 3 used in this study. The samples are grown by UHV-CVD. *Note*: T$_s$ and GR refers to substrate temperature and growth rate, respectively

liquid nitrogen cooled Ge detector in conjunction with a standard lock-in technique. The structural characteristic of the samples, such as interface roughness, layer thickness and Ge concentration were characterized using cross-sectional transmission electron microscopy (XTEM) and high resolution x-ray diffraction (HRXRD).

Results and discussion

Figure 2 shows the x-ray rocking curves of samples 1–3. The sharp peaks in the rocking curves arise from the Si substrate. The experimental rocking curves were compared with dynamical simulation to determine the physical parameters of the structures. For sample 1, the simulation was performed based on a 10-period

5.7 nm-thick $Si_{0.66}Ge_{0.34}$ QW and 40 nm-thick Si barrier stack. For sample 2, the simulation was performed based on a 5.7 nm-thick $Si_{0.66}Ge_{0.34}$ QW, 4 nm-thick Si barrier and 5.7 nm-thick $Si_{0.66}Ge_{0.34}$ QW. Finally for sample 3, the simulation was performed based on a 5-period 5.6 nm-thick $Si_{0.66}Ge_{0.34}$ QW, 2 nm-thick Si barrier, and 5.6 nm-thick $Si_{0.66}Ge_{0.34}$ QW and 40 nm-thick Si barrier stack. As shown in the figure, the experimental XRD data of the samples are well reproduced by the dynamical simulation. However, compared with the simulated curves, certain satellite peaks are missing in the experimental results. This is due to the imperfect interfaces between the QWs and barriers, which are confirmed by XTEM examination of the samples as shown in Fig. 3. The dark regions correspond to the SiGe QWs, while the relatively bright regions correspond to the Si barriers. The XTEM micrographs show that the high degree of strain (up to 1.5%) between the QWs and barriers gave rise to substantial thickness variations (the roughness is about 7 Å) in the QWs and barriers.

The thickness variations in the QWs and barriers result in the relatively weak and broad PL spectra of the SiGe QWs observed in samples 1–3, as shown in Fig. 4. In the figure, NP, TA and TO refers to no-phonon, transverse-acoustic phonon-assisted and transverse-optical phonon-assisted transitions, respectively [11]. The full-width at half maximum (FWHM) of the PL signal of sample 1 is about 40 meV (as marked in Fig. 4). The contribution to the FWHM of this signal by interface roughness (ΔL) could be estimated by the following equations [12, 13]:

$$\Delta E = \left[\frac{dE_{1e}}{dL} + \frac{dE_{1hh}}{dL}\right] \Delta L \tag{1}$$

(W) and barrier (B), and ΔE_c and ΔE_v are the band offsets of the conduction and valence bands, respectively. Hence, out of the total FWHM of 40 meV, 13.1 meV is contributed by the interface roughness between the QW and barrier layers. The large difference of ~27 meV between the estimated and measured FWHM values could be due to the presence of interface defects, which are caused by the partial strain relaxation due to lattice mismatch at the interface.

In Fig. 4, the PL peaks shift to lower energy following decrease in the barrier thickness. This is due to the effect of interwell coupling between the two symmetrically-aligned wells caused by the wavefunction penetration across the Si barrier. When two quantum wells are brought close enough, such as the case of samples 2 and 3, the energy states in both the conduction and valence bands are split into symmetric (S) and anti-symmetric (A) states due to the coupling effect (as shown in the inset of Fig. 4). In the valence band, both the heavy hole (HH) and light hole (LH) states are split. However, the energy of the HH S-state is higher than that of the LH S-state (the difference is about 60 meV in our calculation). Hence, the observed luminescence should be attributed to the optical transition between the S-states of electrons and the HH states in the valence band. The energy of HH S-state is higher than that of the HH state before split (the difference is about 15 meV in our calculation). Therefore the NP transition energy reduces in the presence of coupling effect. This explains the observation that red shift of the PL peak energy follows a reduction in barrier thickness. Note that the band energy changes in the conduction band could be ignored, because the band offsets in the conduction bands in our samples are very small.

$$\frac{dE_{1e}}{dL} = \frac{E_{1e}}{\frac{L}{2} + \frac{\hbar}{\sqrt{2m_e^B(\Delta E_c - E_{1e})}}\cos^2\left(\frac{L}{2}\sqrt{\frac{2m_e^W E_{1e}}{\hbar^2}}\right) + \frac{\hbar}{\sqrt{8m_e^W E_{1e}}}\sin\left(L\sqrt{\frac{2m_e^W E_{1e}}{\hbar^2}}\right)} \tag{2}$$

$$\frac{dE_{1hh}}{dL} = \frac{E_{1hh}}{\frac{L}{2} + \frac{\hbar}{\sqrt{2m_{hh}^B(\Delta E_v - E_{1hh})}}\cos^2\left(\frac{L}{2}\sqrt{\frac{2m_{hh}^W E_{1hh}}{\hbar^2}}\right) + \frac{\hbar}{\sqrt{8m_{hh}^W E_{1hh}}}\sin\left(L\sqrt{\frac{2m_{hh}^W E_{1hh}}{\hbar^2}}\right)} \tag{3}$$

where L is the QW width and E_{1e} and E_{1hh} are the energy values of the first energy state in the conduction and valence bands. m_e^B, m_e^W, m_{hh}^B and m_{hh}^W are the effective mass of the electron and heavy hole in the QW

In sample 1, since the thickness of the Si barrier is 40 nm, the QWs in this sample should be effectively isolated from each other. This being the case, it should have similar characteristic as a single QW (SQW) with
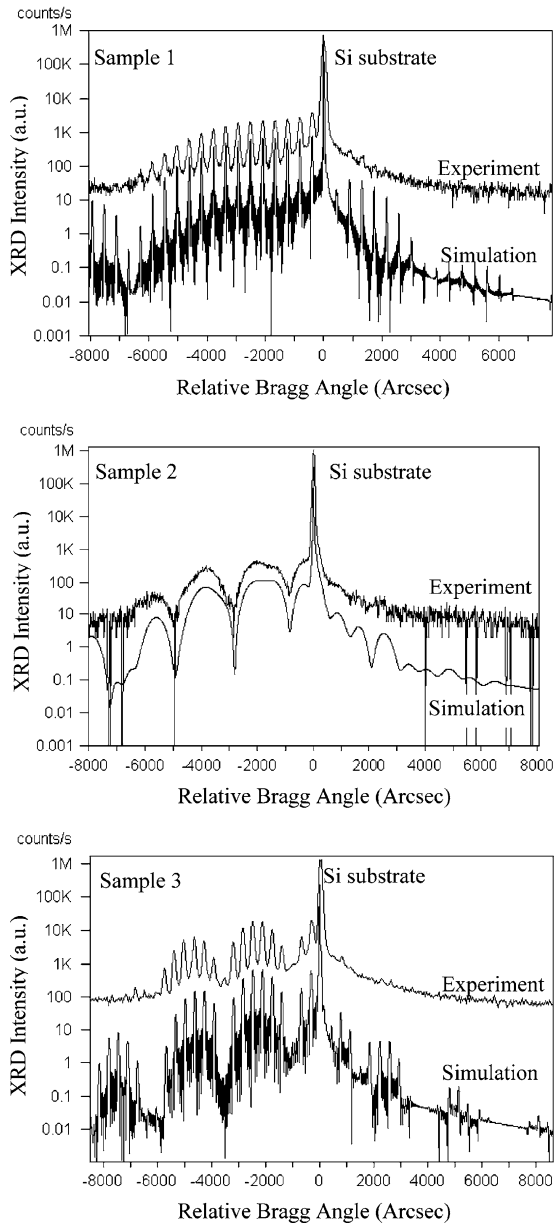
Fig. 2 Experimental and simulated x-ray rocking curves of the symmetric (0 0 4) reflection for samples 1, 2 and 3 (from top to bottom)

Fig. 3 XTEM micrographs of (**a**) sample 1, (**b**) sample 2 and (**c**) sample 3. Dark and bright regions correspond to the SiGe QW and Si barrier layers, respectively

the same QW width and Ge composition. The band structure of a strained $Si_{0.66}Ge_{0.34}$ SQW grown on Si substrate is shown in Fig. 5. For a strained $Si_{1-x}Ge_x$ layer (x < 0.4) grown on Si substrate, the indirect bandgap E_g at 4.2 K can be expressed as [14]:

$$E_{g,SiGe}(x) = 1.17 - 0.896x + 0.396x^2 \text{ (eV)} \tag{4}$$

The valence band discontinuity is given by the following equation [15]:
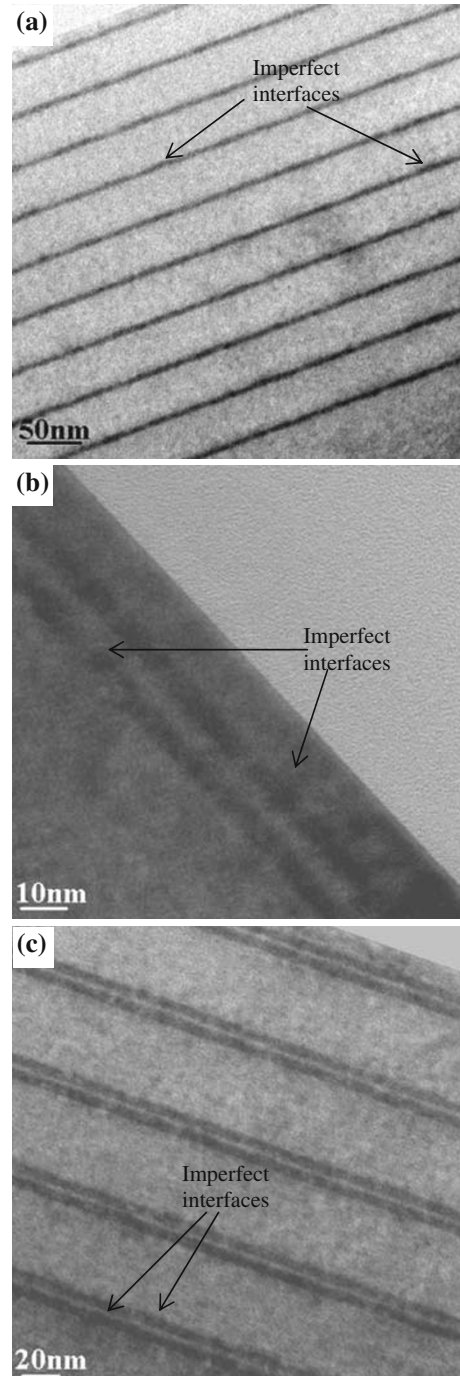
$$\Delta E_v = 0.74x \text{ (eV)} \tag{5}$$

Hence the conduction band offset could be obtained by:

$$\Delta E_c = -0.156x + 0.396x^2 \tag{6}$$

If the value of ΔE_c is positive, the band alignment is type-II, otherwise the band alignment is type-I.
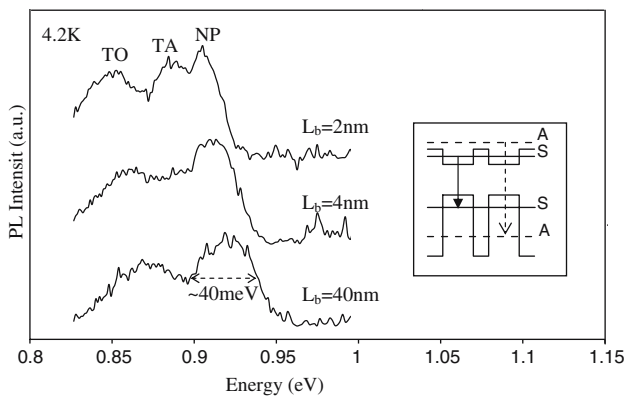
Fig. 4 PL spectra of samples 1, 2 and 3 (from bottom to top) measured at 4.2 K. The barrier thickness (L_b) of samples 1, 2 and 3 are 40, 4 and 2 nm, respectively. Inset shows the band structure of the CQWs. S and A represent the symmetric and anti-symmetric states, respectively [9]
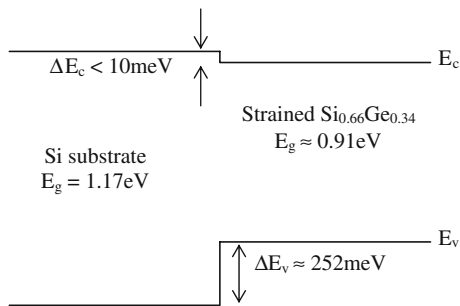

Fig. 5 Schematic diagram of the band structure of a strained $Si_{0.66}Ge_{0.34}$ layer grown on Si substrate. Note: E_g is the bandgap, E_c, E_v, is the conduction and valence band, respectively, and ΔE_c, ΔE_v is the conduction band and valence band discontinuities, respectively. The values of the energies shown in the figure are calculated at 4.2 K

According to the work of Van de Walle and Martin [15, 16], the energy splitting of the valence band is given by the following equations:

$$\Delta E_{v,1} = -\frac{1}{6}\Delta_0 + \frac{1}{4}\delta E + \frac{1}{2}\left[\Delta_0^2 + \Delta_0\delta E + \frac{9}{4}(\delta E)^2\right]^{1/2} \tag{7}$$

$$\Delta E_{v,2} = \frac{1}{3}\Delta_0 - \frac{1}{2}\delta E \tag{8}$$

$$\Delta E_{v,3} = -\frac{1}{6}\Delta_0 + \frac{1}{4}\delta E - \frac{1}{2}\left[\Delta_0^2 + \Delta_0\delta E + \frac{9}{4}(\delta E)^2\right]^{1/2} \tag{9}$$

where Δ_0 is the spin-orbital splitting. For strain along the (001) direction, δE is equal to $2b(\varepsilon_\perp - \varepsilon_{//})$, where b

is the uniaxial deformation potential for tetragonal strain. $\Delta E_{v,1}$, $\Delta E_{v,2}$ and $\Delta E_{v,3}$ represent the band energy offsets of the light, heavy and split-off band at the valence band, respectively. The energy splitting of the conduction band is given by the following equations:

$$\Delta E_c^{001} = \frac{2}{3}\Xi_u^\Delta\left(\varepsilon_\perp - \varepsilon_{//}\right) \tag{10}$$

$$\Delta E_c^{100,010} = -\frac{1}{3}\Xi_u^\Delta\left(\varepsilon_\perp - \varepsilon_{//}\right) \tag{11}$$

where Ξ_u^Δ is the uniaxial strain deformation potential for the conduction band. Hence, the theoretical NP energy value of sample 1 could be estimated by the above equations. The estimated value is 934 meV, which is in good agreement with the measured value of 920 ± 5 meV, and is consistent with the theoretical value of 923.7 meV calculated by the 6 + 2-band $k \cdot p$ method. The parameters used for the calculation are obtained by linear interpolation between the parameters of Si and Ge (as shown in Table 1) [17, 18].

For samples 2 and 3, the theoretical calculations of the band structures are more complex, when taking interwell coupling effects in these two samples into consideration. By employing calculations based on the 6 + 2-band $k \cdot p$ method [19, 20], the calculated NP transition energy values of samples 2 and 3 are 908.4 meV and 906 meV, respectively. These values are in close agreement with the measured value of 907 ± 3 meV and 904 ± 2 meV, respectively. The consistency between the measured and theoretical values further confirms that the interwell coupling effect is present in samples 2 and 3. Therefore, inter-subband transition, which is the essential phenomenon

Table 1 Parameters used in the calculations. *Note*: a_c, a_v and b are obtained from Ref. 15 and other parameters are obtained from Ref. 18

Parameters	Si	Ge
Lattice constant a_0 (Å)	5.431	5.658
Spin-orbit splitting energy Δ_0 (eV)	0.044	0.296
Optical matrix parameter E_p (eV)	21.6	26.3
Deformation potential constant a_c (eV)	4.88	2.55
Deformation potential constant a_v (eV)	2.46	2.55
Shear deformation potential b (eV)	–2.33	–2.08
Uniaxial deformation potential Ξ_u^Δ (eV)	9.29	10.20
Elastic constant c_{11} (Mbar)	1.675	1.315
Elastic constant c_{12} (Mbar)	0.65	0.494
Luttinger parameter γ_1	4.22	13.4
Luttinger parameter γ_2	0.39	4.25
Luttinger parameter γ_3	1.44	5.69
Longitudinal mass m_l^* (m_0)	0.9163	0.7991
Transverse mass m_t^* (m_0)	0.1905	0.2

in QC emitters, could be obtained in these samples. This will be verified in the future experiments.

Conclusions

In summary, the interwell coupling effect in Si/$Si_{0.66}Ge_{0.34}$ CQWs structures grown by UHV-CVD was investigated using low temperature PL measurements. Red shift of PL peak energy caused by interwell coupling was observed following a reduction in barrier thickness. Variations in the QW and barrier thickness and possibly defects in the as-grown material could have contributed to the relatively broad PL signals from the samples. The band structure model of the Si/SiGe heterostructure was validated by comparing theoretical calculations based on the 6 + 2-band $k \cdot p$ method with experimental values of the no-phonon PL peak. The close agreement between the measured data and theoretical calculations confirms the presence of the interwell coupling effect in samples with narrow barriers. The results from this work are useful for future growth and design of Si/SiGe QC emitters.

References

1. G. Franzo, F. Priolo, S. Coffa, A. Polman, A. Carnera, Appl. Phys. Lett. **64**(17), 2235 (1994)
2. L. Pavesi, L. Dal Negro, C. Mazzoleni, G. Franzo, F. Priolo, Nature **408**(6811), 440 (2000)
3. S.G. Cloutier, P.A. Kossyrev, J. Xu, Nat. Mater. **4**, 887 (2005)
4. G. Dehlinger, L. Diehl, U. Gennser, H. Sigg, J. Faist, K. Ensslin, D. Grützmacher, E. Müller, Science **290**, 2277 (2000)
5. I. Bormann, K. Brunner, S. Hackenbuchner, G. Zandler, G. Abstreiter, S. Schmult, W. Wegscheider, Appl. Phys. Lett. **80**(13), 2260 (2002)
6. R. Bates, S.A. Lynch, D.J. Paul, Z. Ikonic, R.W. Kelsall, P. Harrison, S.L. Liew, D.J. Norris, A.G. Cullis, W.R. Tribe, D.D. Arnone, Appl. Phys. Lett. **83**(20), 4092 (2003)
7. J. Faist, F. Capasso, D.L. Sivco, C. Sirtori, A.L. Hutchinson, A.Y. Cho, Science **264**, (1994) 553
8. S. Fukatsu, H. Yoshida, N. Usami, A. Fujiwara, Y. Takahashi, Y. Shiraki, R. Ito, Thin Solid Films **222**, 1 (1992)
9. S. Fukatsu, Y. Shiraki, Appl. Phys. Lett. **63**(17), 2378 (1993)
10. S. Fukatsu, Solid State Electron. **37**, 817 (1994)
11. J.C. Sturm, H. Manoharan, L.C. Lenchyshyn, M.L.W. Thewalt, N.L. Rowell, J.-P. Noël, D.C. Houghton, Phys. Rev. Lett. **66**(10), 1362 (1991)
12. M.A. Herman, D. Bimberg, J. Christen, J. Appl. Phys. **70**, R1(1991)
13. P. Acosta-Díaz, O. Cano-Aguilar, F.L. Castillo-Alvarado, M. Meléndez-Lira, M. López-López, Superficies Y Vacío **12**, 39 (2001)
14. D.J. Robbins, L.T. Canham, S.J. Barnett, A.D. Pitt, P. Calcott, J. Appl. Phys. **71**(3), 1407 (1992)
15. C.G. Van de Walle, R.M. Martin, Phys. Rev. B **34**(8), 5621(1986)
16. C.G. Van de Walle, Phys. Rev. B **39**(3), 1871(1989)
17. D.J. Paul, Scmicond. Sci. Technol. **19**, R75 (2004)
18. O. Madelung, M. Schultz, H. Weiss (ed.), *Semiconductors, Physics Group IV Elements and III–V Compounds*, Landolt-Börnstein, New Series Group III, vol 17 (Springer-Verlag, New York, 1982), part a
19. Y.X. Dang, W.J. Fan, S.T. Ng, S.F. Yoon, D.H. Zhang, J. Appl. Phys. **97**(10), 103718 (2005)
20. Y.X. Dang, W.J. Fan, F. Lu, H. Wang, D.H. Zhang, S.F. Yoon, J. Appl. Phys. **99**(7), 076108 (2006)